

Alma Mater Studiorum Università di Bologna
Archivio istituzionale della ricerca

Radionuclide concentration and radon exhalation in new mix design of bricks produced reusing NORM by-products: The influence of mineralogy and texture

This is the final peer-reviewed author's accepted manuscript (postprint) of the following publication:

Published Version:

Coletti, C., Brattich, E., Cinelli, G., Cultrone, G., Maritan, L., Mazzoli, C., et al. (2020). Radionuclide concentration and radon exhalation in new mix design of bricks produced reusing NORM by-products: The influence of mineralogy and texture. CONSTRUCTION AND BUILDING MATERIALS, 260, 1-13 [10.1016/j.conbuildmat.2020.119820].

Availability:

This version is available at: <https://hdl.handle.net/11585/763071> since: 2020-06-25

Published:

DOI: <http://doi.org/10.1016/j.conbuildmat.2020.119820>

Terms of use:

Some rights reserved. The terms and conditions for the reuse of this version of the manuscript are specified in the publishing policy. For all terms of use and more information see the publisher's website.

This item was downloaded from IRIS Università di Bologna (<https://cris.unibo.it/>).
When citing, please refer to the published version.

(Article begins on next page)

This is the final peer-reviewed accepted manuscript of:

COLETTI, C., BRATTICH, E., CINELLI, G., CULTRONE, G., MARITAN, L., MAZZOLI, C., MOSTACCI, D., TOSITTI, L., SASSI, R., 2020. RADIONUCLIDE CONCENTRATION AND RADON EXHALATION IN NEW MIX DESIGN OF BRICKS PRODUCED REUSING NORM BY-PRODUCTS: THE INFLUENCE OF MINERALOGY AND TEXTURE. CONSTRUCTION AND BUILDING MATERIALS 260, 119820.

The final published version is available online at:

[10.1016/j.conbuildmat.2020.119820](https://doi.org/10.1016/j.conbuildmat.2020.119820)

Terms of use:

Some rights reserved. The terms and conditions for the reuse of this version of the manuscript are specified in the publishing policy. For all terms of use and more information see the publisher's website.

This item was downloaded from IRIS Università di Bologna (<https://cris.unibo.it/>)

When citing, please refer to the published version.

1 **Radionuclide concentration and radon exhalation in new mix design of bricks produced reusing**
2 **NORM by-products: the influence of mineralogy and texture.**

3
4
5
6
7 Chiara Coletti¹, Erika Brattich², Giorgia Cinelli³, Giuseppe Cultrone⁴, Lara Maritan¹, Claudio
8
9
10 Mazzoli¹, Domiziano Mostacci⁵, Laura Tositti⁶, Raffaele Sassi¹

11
12
13
14 ¹ Department of Geosciences, University of Padova, Via Gradenigo 6, 25131 Padova, Italy

15
16
17 ² Department of Physics and Astronomy, University of Bologna, via Irnerio 46, 40126 Bologna, Italy

18
19 ³ European Commission, Joint Research Centre (JRC), Via Enrico Fermi 2749, 21027 Ispra VA, Italy

20
21
22 ⁴ Department of Mineralogy and Petrology, Faculty of Science, University of Granada, Fuentenueva
23
24 s/n, 18002 Granada, Spain

25
26
27 ⁵ Department of Industrial Engineering, University of Bologna, Via dei Colli 16, 40136 Bologna,
28
29 Italy

30
31
32 ⁶ Department of Chemistry “G. Ciamician”, University of Bologna, Via Selmi 2, 40126 Bologna,
33
34 Italy

35
36
37
38
39 **Abstract**

40
41 Many industrial by-products contain Naturally Occurring Radioactive Materials (NORM) that
42
43 normally represent a cost in terms of monitoring, risk management and storage. When included in
44
45 new mix designs of bricks, these materials may become a valuable sustainable resource. Before
46
47 marketing, companies involved in development and commercialization of these new building
48
49 materials ensure safety related to radiation, usually by assessing radon-related risk. According to the
50
51 Council Directive 2013/59/Euratom, both raw materials and final products used in building
52
53 constructions need to be tested for activity concentration. The present work explores the radionuclide
54
55 concentration and the radon exhalation of bricks obtained recycling different types of potentially
56
57 radioactive wastes: i) trachyte as by-product resulting from quarrying operations, and ii) two different
58
59
60
61
62
63
64
65

27 types of industrial sludge derived from ceramic tiles industry. Raw materials were studied to foresee
1
28 any potential radioactive risk derived from their use as secondary raw materials, while bricks were
3
4
529 investigated to assess the influence of mineralogy and texture on their radioactive properties and their
6
730 effective radon-risk. The results obtained here show that, although radon emanation in bricks is
8
9
1031 primarily determined by radionuclide concentration in the raw materials, textural features
11
1232 significantly affect radon mobility and exhalation.
13
14
1533

16
1734 Key words: Bricks; Radioactivity; Radon; Building materials; Industrial by-products.
18
19
2035
21

2236 **Introduction**

23
2437 Building materials produced from rocks and sediments (clay, sand, gravel and soils) contain natural
25
26
2738 radioactive elements at highly variable concentration levels and can constitute Naturally Occurring
28
2939 Radioactive Materials (NORM) [1-11]. Natural radioactivity of building materials contributes to the
30
31
3240 mean annual radiation dose to population both in terms of external irradiation directly emitted from
33
3441 the material and of internal exposure related to the radon exhaled [12-14]. External radiation exposure
35
3642 is determined by direct gamma radiation from external sources, and can be assessed from the activity
37
38
3943 concentrations of radium (^{226}Ra), thorium (^{232}Th), and potassium (^{40}K). Internal radiation exposure
40
4144 by building materials. is caused by inhalation of gaseous radon, released from pores and fractures in
42
43
4445 the material itself [15-17]. NORM in building materials are mainly associated with the radioactive
45
4646 families of ^{238}U , ^{232}Th , and the primordial ^{40}K , the radioactivity from the ^{235}U family being negligible
47
48
4947 as compared to ^{238}U on the basis of their relative isotopic abundance. Particular attention should be
50
5148 paid to radon (^{222}Rn), thoron (^{220}Rn), and their daughters, whose inhalation enhances the risk of
52
53
5449 bronchial and lung cancer [18,19]. NORM include several materials such as bulk rocks used as
55
5650 dimension stones, whose radioactivity is tightly connected with their petrography, or bricks, tiles,
57
5851 cement, concrete and other materials manufactured from mixtures of geological materials such as
59
60
61
62
63
64
65

52 clay, sand, gravel and other components from local or remote sources. Activity concentration of these
1
253 components will contribute to the average radioactivity of the final building material.
3
4
54 In the last decades, the amounts of waste from human activities and by-products from the industry
6
755 has been constantly increasing, affecting disposal costs and rising dramatic environmental concerns.
8
9
1056 In addition, our society is facing a progressive shortage of geo-resources as virgin raw materials.
11
1257 Thus, industry searches for alternative secondary raw materials, including the recycling of both
13
1458 wastes and by-products. This trend is partly motivated by an increasing awareness of the need for
15
16
1759 green strategies [20-28], and partly by the perspective of reducing costs, especially in the production
18
1960 of building material. Although mitigating the impact on the environment by reducing primary geo-
20
21
2261 resources exploitation, and often even improving their properties, these products are required to
23
2462 undergo health risk assessment and fulfil health standards before being commercialised [14,29,30].
25
26
2763 When waste and by-products are incorporated into a newly designed building material, the final
28
2964 product will contain all their original chemical components, including radionuclides, yielding a
30
31
3265 mixture of stable and radioactive components depending on the amounts and composition of the
33
3466 precursor materials employed [31]. Moreover, the texture of the final product may also change during
35
3667 the production process, therefore modifying the permeability of the final product to gases. For
37
38
3968 example, mineralogy and pore structure of bricks may significantly change during firing, depending
40
4169 on the different raw materials used [32]. Building materials containing secondary raw materials may
42
43
4470 potentially expose people to radiation: for this reason, it is necessary to investigate radioactivity on
45
4671 both raw materials and final products [33].
47
48
4972 In Europe, the first attempt to regulate radioactivity of building materials dates back to 1999, when
50
5173 the European Commission released the Radiation Protection 112 [12], a document containing criteria
52
5374 and application rules for dose assessment. In order to estimate exposure from building materials,
54
55
5675 Radiation Protection 112 introduced the index I, calculated from ^{226}Ra , ^{232}Th and ^{40}K activity
57
5876 concentrations experimentally determined by high resolution gamma spectrometry. However, it is
59
60
61
62
63
64
65

77 only in 2014 that the European Union enforced the previous documents into the Council Directive
1
278 2013/59/Euratom [34].
3
4
579 Radiation Protection 112 guidance [12] mandates that “*when industrial by-products are incorporated*
6
780 *in building materials and there is reason to suspect that these contain enhanced levels of natural*
8
9
1081 *radionuclides, the activity concentrations of these nuclides in the final product should be measured*
11
1282 *or assessed reliably from the activities of all component materials*”. Article 75 of the Council
13
14
1583 Directive 2013/59/Euratom [34] encompasses different types of building materials, dividing them
16
1784 into natural materials and materials incorporating residues from processing industries. If the activity
18
1985 concentration index (I) of these residues are below the reference levels imposed by the Council
20
21
2286 Directive 2013/59/Euratom [34], the derived building materials can be used without restriction.
23
2487 In view of a safe re-use in bricks of by-products potentially enriched in natural radioactivity, their
25
26
2788 physical, chemical, mineralogical, and radiological properties should be considered and accurately
28
2989 characterised. The Council Directive 2013/59/Euratom [34] does not provide guidelines to account
30
31
3290 for the specific radon exhalation/emanation contribution from the building materials. This specific
33
3491 issue has been recently reviewed in detail by the COST Action Tu1301 NORM4BUILDING, that
35
3692 contributed to collect and organize available information, and set up operational guidelines for the
37
38
3993 management of all building materials including those containing NORM by-products, and for the
40
4194 formulation of new synthetic ones [14,33]. Radiological aspects in the recycling of by-products in the
42
43
4495 manufacturing of cement, concrete, ceramics, and other construction materials are discussed in
45
4696 Chapter VII of the COST Action Tu1301 NORM4BUILDING [33]. On the contrary, both traditional
47
48
4997 bricks and bricks produced using NORM by-products have been poorly studied and most of the
50
5198 standards that regulate radioactivity [12, 34] addressed gamma radiation rather than radon exhalation
52
5399 and the related control of texture and porosity.
54
55
5600 In this work, we describe the results of an integrated approach aimed at characterizing radioactivity
57
5801 and mineralogy of two series of newly designed bricks obtained from the same base clays, tempered
59
60
6102 with two different types of ceramic sludge and a by-product of quarrying activity, consisting of finely
62
63
64
65

103 fragmented trachyte waste. Both these types of industrial by-products may potentially increase
1
104 radioactivity of the bricks: sludge from ceramic production could contain radioactive elements
3
105 derived from the additives used for specific treatments (e.g. sintering, hardening, whitening) or added
4
6
106 to glaze, such as zircon [36]; trachyte is a volcanic rock characterised by relatively high
8
107 concentrations of radionuclides [37].
9

108 The paper is organised as follows:
11

- 109 - determination of the radioactivity level of bricks as well as of the single raw materials used such as
15
110 base clay and temper from industrial by-products;
18
- 111 - correlation of radioactivity with mineralogical and physical features, to predict radioactivity in
20
112 newly designed building materials when produced using potentially radioactive by-products;
23
- 113 - comparison of the radioactivity and the mineralogy of a set of conventional bricks, the mineralogy,
25
114 texture and mechanical properties of which had been already previously determined [27,30,32,35],
27
115 with the radioactivity and mineralogy of these new products.
30

116 117 **2. Materials**

118 A set of different bricks, and corresponding raw materials, have been analysed. Raw materials include
37
119 four different types of clay, tailings from quarrying activity, two types of sludge from ceramic
40
120 industry, and a dye additive (Table 1). The following clay raw materials provided by the Company
42
121 San Marco-Terreal (Italy) were considered: LG (*Laminato Giallo*, i.e. “Yellow Laminated”), LRS
44
122 (*Laminato Rosa*, “Pink Laminated”), LRSS (*Laminato Rosso*, “Red Laminated”) and LRSSF
47
123 (*Laminato Rosso Forte*, “Intense Red Laminated”). These clays have similar mineralogy but different
49
124 relative abundance of their components, especially carbonates [27]. Two types of industrial by-
52
125 products replacing the traditional temper to produce experimental bricks were characterized: i) two
54
126 types of sludge derived from ceramic industry (samples F and PIR) [35]; ii) a finely fragmented
57
127 trachyte waste produced by quarrying activity (sample TR) at M. Altore, in the Euganean Hills
59

128 Volcanic District (north-eastern Italy) [30]. Furthermore, a Mn-oxide-based dye additive was also
1
2 considered (sample MN), as it is used in one of the commercial bricks here studied (sample N).

3
4
5 The bricks analysed can be grouped in three different categories (Table 1): i) commercial bricks
6
7 (produced by San Marco-Terre); ii) experimental bricks obtained by adding the trachyte waste; iii)
8
9 experimental bricks obtained by adding the two types of sludge from ceramic industry.

10
11
12 The six commercial bricks (samples GP, N, RS, RSS, R6, RCF) are produced by adding 10 wt. % of
13
14 a quartz-rich sand (sample SS) to the different clayey materials (LG, LRS, LRSS, LRSSF) (Table 1).

15
16
17 The mixtures are fired at different temperatures (Table 1), depending on the specific clay used. In
18
19 addition, different proportions of a dye (additive MN) were added to sample N, up to 15 wt. %.

20
21
22 Nine experimental bricks were obtained by tempering the most siliceous clayey material (LRSSF)
23
24 with 5, 10 and 15 wt. % (samples with prefix B5, B10 and B15, respectively) of sand-sized fragments
25
26 of trachyte, and firing each mixture at three different temperatures: 900, 1000, 1100 °C (suffix 9, 10
27
28 and 11, respectively).

29
30
31 Two additional experimental bricks (samples MF and B_PIR) were obtained tempering the most
32
33 carbonate-rich clay (LGP) with 10 wt. % of the two different types of sludge (F and PIR); both
34
35 mixtures were then fired at 1050 °C (same firing temperature as commercial bricks GP and N obtained
36
37 from the same base clay). Types of material and experimental conditions are summarized in Table 1.

38
39
40
41
42

43 44 45 46 **3. Methods**

47
48 The chemical composition of the samples was determined by X-ray fluorescence (XRF) on an S4
49
50 Pioneer (Bruker AXS) spectrometer, with an estimated detection limit of 0.01 wt. % for major
51
52 elements; trace elements, expressed in ppm, have the following analytical detection limits: Zr = 15
53
54 ppm, Rb = 18 ppm; Sr = 20 ppm; Cr 11 = ppm; Zn = 15 ppm; Ni = 1 ppm; Pb = 17 ppm. ZAF method
55
56 was employed for quantitative analysis [38], while the NCS DC 74301 (GSMS-1) standard was used
57
58 for calibration [39].
59
60
61
62
63
64
65

153 X-ray powder diffraction (XRPD) was applied to identify the mineral phases of raw materials and
1
154 fired products. Diffraction data were acquired using a PANalytical X'Pert PRO diffractometer,
2
3
4
155 operating in Bragg-Brentano reflection geometry with CoK α radiation, 40 kV of voltage and 40 mA
5
6
156 of filament current, equipped with an X'Celerator detector. Qualitative analysis of diffraction data
7
8
9
157 was carried out with X'Pert HighScore Plus[®] software (PANalytical) and the PDF-2 database. The
10
11
158 petrographic and textural characteristics of thin sections were examined under a polarized light optical
12
13
14
159 microscope (Olympus DX-50, equipped with a Nikon D7000 digital microphotography system).
15
16
160 Texture and reaction microstructures were examined by Scanning Electron Microscopy (SEM) with
17
18
19
161 a CamScan MX-2500 microscope, coupled with an EDAX Sapphire Si(Li) detector (LEAP+Si(Li)
20
21
22
162 crystal), equipped with a LaB₆ cathode operating at 20 kV and 160 nA.
23
24
163 The distribution of pore-access size (radius range: 0.001-100 μm) was determined by Mercury
25
26
164 Intrusion Porosimetry (MIP) on a Model 9410 Micromeritics Autopore apparatus, which can generate
27
28
29
165 a pressure of 414 MPa. Freshly cut samples of approximately 2 cm³ were oven-dried for 24 hours at
30
31
32
166 110 °C and then analyses.
33
34
167 Nitrogen adsorption was used to determine brick porosity in the range (in diameter) between 0.0002
35
36
168 and 0.3 μm . Sorption isotherms were obtained at 77 K, on a Micromeritics Tristar 3000 in continuous
37
38
39
169 adsorption conditions. Prior to measurement, samples were heated at 130 °C for 24 h and outgassed
40
41
42
170 to 10⁻³ Torr on a Micromeritics Flowprep. Specific surface area of pores was determined by
43
44
171 Brunauer–Emmett–Teller (BET) theory based on the physical adsorption of gas onto the surface of a
45
46
172 solid.
47
48
173 Activity levels of raw material and finite products were evaluated both measuring concentrations of
49
50
51
174 K, U, Th and descendants by XRF, and high-resolution γ -ray spectroscopy. Samples were analysed
52
53
175 with two p-type coaxial Hyper Pure Germanium crystal detectors (HPGe), a PROFILE (Ortec-
54
55
176 Ametek Inc.) with an extended energy range (20–2000 keV) and a conventional GEM model (Ortec-
56
57
177 Ametek Inc.) with an energy range 80-2000 keV. These detectors have relative efficiency of 20% and
58
59
60
178 38%, and resolution (FWHM) at 1332.5 keV of 1.9 keV and 1.8 keV, respectively. Both systems
61
62
63
64
65

179 were calibrated for energy and efficiency using a liquid standard source (Eckert & Ziegler
 180 Multinuclide standard solution 7501) in a jar geometry (diameter = 56 mm; thickness = 10 mm).
 181 Spectra were acquired for 1 day to optimize peak analysis. Spectra were subsequently processed and
 182 analysed with the Gamma Vision-32 software (version 6.07, Ortec-Ametek Inc.) [40]. ^{226}Ra was
 183 determined at 186 KeV correcting the peak area by the ^{235}U interference according to the method
 184 proposed by Gilmore (2008) [41], under the hypotheses of secular equilibrium between ^{226}Ra - ^{238}U
 185 and natural $^{235}\text{U}/^{238}\text{U}$ isotopic ratio. ^{238}U and ^{232}Th were then determined using the emissions of their
 186 radioactive daughters ^{226}Ra and ^{228}Ac .

187 The minimum detectable activity (CR_{MDA}) was calculated according the so-called Traditional
 188 ORTEC method available in GammaVision according to the expression:

$$\text{CR}_{\text{MDA}} = \frac{\frac{100}{\text{SENS}} \cdot \left(\sqrt{2 \cdot B_1 + \frac{2500}{\text{SENS}^2}} + \frac{50}{\text{SENS}} \right)}{\text{LT}}$$

189 where SENS is the Peak Cutoff value (%) on the Analysis tab (40% in this work), B1 is the Peak
 190 background, and LT is the Live Time (sec).

191 Conversion from activity concentration (Bq/kg) to bulk elemental weight fraction was obtained
 192 through the following conversion factors [42]:

194 $1\% \text{ K} = 309.7 \text{ Bq/kg}$

195 $1 \text{ ppm U} = 12.35 \text{ Bq/kg}$

196 $1 \text{ ppm Th} = 4.072 \text{ Bq/kg}$

197 Council Directive 2013/59/Euratom [34] defines the Activity Concentration Index (I) in order to
 198 quantify and regulate the exposure to gamma radiation originating from radionuclides in building
 199 materials:

$$I = C_{\text{Ra}226} / 300 \text{ Bq/kg} + C_{\text{Th}232} / 200 \text{ Bq/kg} + C_{\text{K}40} / 3000 \text{ Bq/kg}$$

201 where C_{Ra} , C_{Th} and C_{K} are the specific activities of ^{226}Ra , ^{232}Th and ^{40}K , respectively, expressed in
 202 Bq/kg. The activity concentration index value of 1 can be used as a conservative screening tool for
 203 identifying materials that may cause the reference level (1 mSv per year) to be exceeded [34].

204 The alpha-index ($I\alpha$) may be used to regulate the exposure to radon originating from radionuclides in
1 building materials [43,44]:

$$206 I\alpha = C_{Ra}/200 \text{ Bq/kg}$$

207 The reference levels of $I\alpha$ and I are 0.5 and 1, respectively [12,34,43].

208 To assess the radiation hazard of the bricks, the radium equivalent activity (Ra_{eq}) was calculated
10 according to the method introduced by Beretka and Methew (1985) [45] with the following equation:

$$210 Ra_{eq} = C_{Ra} + 1.43 C_{Th} + 0.07 C_K \leq 370 \text{ Bq/kg.}$$

211 Radon emanation and exhalation from a porous material in indoor air should be regarded as a
18 combination of different processes and factors. Firstly, the radon emanation derives from the solid-
19 phase lithology and its characteristic naturally occurring radioactivity. Secondly, since radon atoms
20 recoil and migrate into the pore space, texture and physical features can sensibly affect exhalation.

215 Radon exhalation from the investigated materials was measured by electrets. To this scope, brick
26 samples were cut into cubes (edge = 5 cm) to obtain a measurable external surface. Each sample was
27 introduced in suitable airtight bottles (volume = 0.00372 m³) containing two electrets in SST
31 configuration [Kotrappa]; prior to analysis, radon blank was checked in the closed bottle in the
32 absence of sample. For each sample a parallel measurement with an empty bottle was carried out for
33 background radon subtraction under the same environmental conditions. After tightly sealing the
34 bottles, radon exhalation was allowed over a suitable time (5-7 days); eventually the bottles were
35 opened and electrets retrieved and read, and the experiment repeated. The final exhalation value was
36 taken as the average of two subsequent readings. The radon exhalation rate (Q_A) was then evaluated
37 as follows:

$$225 Q_A \left[\frac{Bq}{d} \right] = \frac{V\lambda}{1 - \frac{1 - e^{-\lambda T}}{\lambda T}} [\langle C \rangle_{sample} - \langle C \rangle_{blank}]$$

226 where λ is the decay constant of ²²²Rn (0.18145 d⁻¹), T the measurement time in days, V the free
57 volume inside the bottle, C the radon concentration in Bq/m³ and the angular brackets indicate
58 average over time (T).
59
60
61
62
63
64
65

229 Finally, specific surface exhalation rate (Ea) is calculated dividing Q_A by the sample surface S in
1
230 square meters:

$$231 \quad Ea \left[\frac{Bq}{d \ m^2} \right] = \frac{Q_A}{S}.$$

232 The radon release per unit mass of the material, specific mass exhalation rate (Em), can be calculated
9
233 dividing Q_A by the mass m in kilograms of the sample:

$$234 \quad Em \left[\frac{Bq}{d \ kg} \right] = \frac{Q_A}{m}.$$

235 According to Stoulos et al. (2003) [13] and Righi and Bruzzi (2006) [44], the radon emanation
17
236 coefficient (η), representing the percentage of radon produced from grains and free in porous system,
19
20
237 can be also defined as follows:

$$238 \quad \eta = Q_A / C_{Ra} \ m \ \lambda_{Rn}$$

239 where Q_A is the measured radon exhalation rate (Bq/d), C_{Ra} the ^{226}Ra content (Bq/kg), λ_{Rn} the ^{222}Rn
27
240 decay constant (1/d), and m is the mass of the sample (kg).

241 Data obtained from the previously described analytical methods, were statistically treated according
31
32
242 to multivariate approaches, consisting in the cluster analysis (CA) and principal component analysis
34
35
243 (PCA), using Statgraphics® Centurion XVI software package. CA represents an optimal approach
36
37
244 for the management of chemical data, since it can describe the natural structure of the dataset and
38
39
245 homogeneous subsets of samples (defined as clusters), which differ from the others to some extent,
41
42
246 expressed by the dissimilarity level. PCA is a multivariate approach which converts a dataset
43
44
247 originally described by numerous variables, possibly correlated, into a dataset expressed new
45
46
248 variables (called principal components), which emphasises the maximum variability among the
47
48
49
249 samples. PCA was performed on the chemical data to evaluate the elements mainly affecting the
51
52
250 differences between bricks, and it was also applied considering the physical parameters (density,
53
54
251 porosity, surface area) as well as the those related to the radiation activity (I , $I\alpha$, Ea , Em , C_{Ra}) in order
55
56
252 to define which of these variables mainly contribute to describe the differences among the bricks, and
57
58
253 to identify possible correlations between various parameters. These statistical approaches, therefore,
59
60
61
62
63
64
65

254 were used to better interpret the possible relationships between the physical, compositional and
1 structural parameters of the bricks with a special attention to the radon-related effects.
255

256

257 **4. Results**

258 **4.1 Raw materials**

259 **4.1.1 Chemical and mineralogical characterization**

260 Chemical composition of clayey materials shows significant differences in CaO and MgO suggesting
14 variable content in carbonates (see Table 2). In particular, samples LRS and LG have both higher
15
16
261 concentrations of these oxides and Loss on Ignition (LOI) than LRSS and LRSSF. This agrees with
18
19
262 the mineralogical composition (Table 3) which indicates that they are illite-chlorite carbonate-rich
20
21
263 clays, with significant amounts of calcite and dolomite.
22
23
264

265 Trachyte (sample TR) is rich in Na₂O and K₂O (Table 2; Na₂O + K₂O ~ 10 wt. %), consistently with
26
27
28
266 the abundance of anorthoclase (an alkali feldspar) and plagioclase, associated with minor amounts of
29
30
31
267 biotite and quartz (Table 3) (see Coletti et al., 2018 [30], and also data referring to M. Altore trachyte
32
33
34
268 in Germinario et al., 2018 [46]); zircon and magnetite occur as accessory minerals as recognised
35
36
37
269 under optical microscope, and account for the Zr (559 ppm) and Fe₂O₃ (3.26%) contents (Table 2).

38
39
270 Sludge materials F and PIR are rich in silica and alumina (Table 2). Quartz and feldspar dominate
40
41
42
271 their mineralogy (Table 3). Sludge F is characterized by mullite and amorphous phase (Table 3) [35],
43
44
272 suggesting an origin from ceramic production in which the firing process reached temperatures above
45
46
47
273 900 °C, when mullite starts to form from illite-muscovite and/or kaolinite breakdown [47] and
48
49
274 sintering occurs. Sludge PIR contains higher amounts of feldspars (both alkali-feldspar and
50
51
52
275 plagioclase), illite and minor amounts of carbonates, as evidenced by the content in CaO and from
53
54
55
276 LOI (2.19 and 4.35 wt. %, respectively; Table 2), and by the presence of calcite reflections in the
56
57
58
277 diffraction pattern (Fig. 1S). This sample also contains relatively high amounts of Zn, Cr and Sr
59
60
61
278 (4915, 2201 and 567 ppm, respectively). These elements are diagnostic of ceramic manufacturing
62
63
64
279 applied to confer specific physical and aesthetical characteristics to the final material body and
65

280 surface: in particular, ZnO is generally used in ceramics as a fluxing agent, Cr to obtain a wide variety
1
281 of different hues, while Sr produces matte glazes [48]. The high amount of Zr both in sludge F and
2
3
4
282 PIR (1583 and 7157 ppm, respectively) is probably related to the wide use of this element in the
5
6
283 ceramic industry both for tile enamel whitening and as a structural component; however, its use has
7
8
284 been strongly reduced in recent times, to avoid its excessive concentration in NORM [48]. PIR
9
10
11
285 presents also moderate amounts of Pb (77 ppm). In the past, Pb has been used as melting agent;
12
13
14
286 nowadays it is mainly used in the production of glaze.
15
16

287 Sample MN is a Mn-oxide (Mn_2O_3 ; hausmannite) and is used as a dye (added to the raw materials in
17
18
19
288 ~15 wt. %) to obtain dark-grey coloured bricks [27].
20
21
22
289

290 **4.1.2 Natural radioactivity**

25

291 Table 4 reports the activity concentration of ^{226}Ra , ^{232}Th and ^{40}K in the raw materials. The measured
26
27
28
292 values on clay span over a range between 29 Bq/kg and 50 Bq/kg for ^{226}Ra , between 34 Bq/kg and 59
29
30
31
293 Bq/kg for ^{232}Th , and between 29 Bq/kg and 50 Bq/kg for ^{40}K . These values are consequently reflected
32
33
294 in the correlated I value (Table 4), providing a minimum of 0.47 for clay LG and a maximum of 0.70
34
35
295 for clay LRSS, in both cases below the recommended value of 1 [34].
36
37

396 Also, α -indexes of clayey materials have all values below the recommended value ($I\alpha \leq 0.5$, Table 4)
38
39
40
41
297 [12], with the maximum value registered for clay LRSS ($I\alpha = 0.25$).
42

298 Among the industrial by-products, F shows very low ^{226}Ra activity concentration with values below
43
44
45
46
47
48
49
300 values. TR has 52 Bq/kg of ^{226}Ra and shows a very high value of ^{40}K (1210 Bq/kg), approximately
50
51
301 twice as much as the other samples, owing to the abundance of alkali feldspars in trachyte (Table 3),
52
53
302 which is naturally characterised by a relatively high radioactivity [37].
54

303 Sludge PIR has the highest activity concentration value of ^{226}Ra (120 Bq/kg, Table 4), responsible
55
56
57
304 for the high $I\alpha$ value (0.60, Table 4), probably connected to the high content in Zr, and supposedly in
58
59
60
305 other high-field-strength elements (HFSE) such as U and Th [49]. Dye additive MN has very low
61
62
63
64
65

306 values of activity concentration (Table 4), below minimum detectable activity for all the analysed
1
307 elements. The highest Ra_{eq} have been detected for samples TR and PIR (216 Bq/kg and 219 Bq/kg,
3
4
308 respectively), much higher than those of the clayey materials, quartz-rich sand, and of the other by-
6
309 products, with values between 30 Bq/kg and 189 Bq/kg (Table 4). This is in agreement with activity
8
310 concentration of the critical radionuclides in the different raw materials, determining slightly higher
10
11 concentration levels than average NORM.
13

14
15

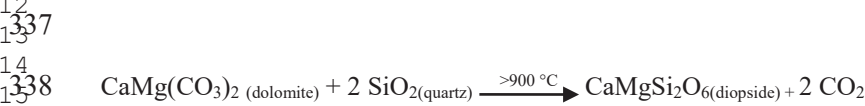
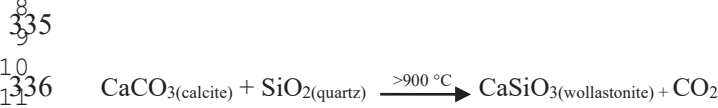
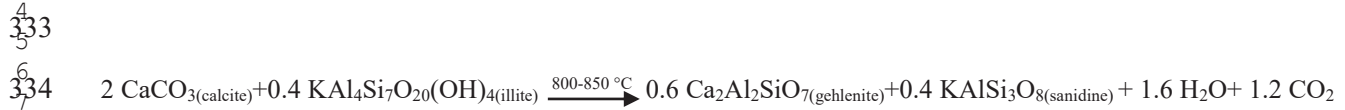
16 4.2 Bricks

17 4.2.1 Chemical composition and mineralogy

18
19
20
21
22 215 The chemical composition of the investigated bricks (Table 2) is consistent with that of the clay
23
24 216 materials used and the temper added (Table 1). The dendrogram of figure 1a reports the hierarchical
25
26
27 217 cluster analysis of the chemical composition performed on XRF data (Table 2). It shows that bricks
28
29 218 GP and FM produced using a carbonate-rich clay (LG) are clustered together (cluster 1) and separated
30
31 219 from the two bricks N and B_PIR produced using the same clay, but obtained by adding the by-
32
33
34 220 products MN and PIR, respectively, which appear as isolated outliers (Fig. 1a) for the higher MnO,
35
36
37 221 Zr and Zn contents, respectively (score and loading plot in Fig. 1b, Table 2). Bricks obtained using
38
39 222 low-Ca clays (LRSS and LRS) form a distinct cluster (cluster 2) (Fig. 1a), whereas those produced
40
41 223 using clay LRSSF group all together in cluster 3 (Fig. 1a). These latter were obtained adding to the
42
43
44 224 base clay a quartz or trachyte sand, respectively; despite the different chemical composition of the
45
46 225 added temper, these bricks group together and are separated from all the others for the higher content
47
48
49 226 in SiO_2 , Na_2O , Fe_2O_3 , P_2O_5 as well as of Ni.

50
51 227 From a mineralogical point of view, the commercial bricks can be distinguished on the basis of the
52
53 228 used clayey materials, temper/additive and firing temperature (Table 3). The new minerals formed at
54
55
56 229 temperature above 800 °C are the result of carbonates (calcite and dolomite) and illite decomposition
57
58
59 230 and their sub-solidus reactions with quartz and feldspar grains. These phases form reaction rims and
60
61
62
63
64
65

331 often display non-stoichiometric compositions. Nonetheless, the main reactions taking place at the
1
332 grain boundaries can be described as follows [22,23,50]:
3



339
340 Brick N contains bustamite $\text{CaMnSi}_2\text{O}_6$, a member of the wollastonite group, isomorphic with
20
341 wollastonite, which developed from the sub-solidus reaction between hausmannite, calcite and quartz
22
342 [35]:
24



344 Brick R6, instead, shows a completely different mineralogy, characterised by persistence of clay-
29
345 forming minerals such as illite, chlorite, and still showing carbonates (calcite and dolomite) because
32
346 fired at 600 °C, thus below their breakdown temperature [27,47,51] (Table 3).
34

347 Bricks obtained from the addition of the two types of sludge (F and B_PIR) are very similar under a
36
348 mineralogical viewpoint to the commercial brick GP, also manufactured using the same carbonate-
39
349 rich clay LG (Table 3), being all enriched in wollastonite and diopside.
41

350 All the experimental bricks obtained by adding trachyte waste to the LRSSF clay display similar
44
351 mineralogical composition, with the occurrence of newly formed silicate phases. Diopside is present
46
352 in small amounts, being the raw clay (LRSSF) very poor in dolomite, while gehlenite is abundant and
49
353 its amount increases as a function of increasing firing temperatures (Table 3). Although firing
51
354 temperatures always exceed typical dolomite and calcite decarbonation temperatures (750 and 850
53
355 °C, respectively), small amounts of calcite survived decomposition as shown in the diffraction
56
356 patterns of the bricks fired at 900 and 1000 °C, while dolomite completely disappeared. Moreover,
58
357 the small amount of illite observed in bricks fired at 1000 °C indicates that amorphisation was not
61
62
63
64
65

358 complete at this temperature. This may also be connected to inhomogeneity in the temperature
1
359 distribution within the kiln, which could have determined the survival of structural domains of
3
360 minerals generally destructured at slightly lower temperatures than firing temperature [30] or as
4
6
361 consequence of non-total amorphisation of illite. Furthermore, biotite in these bricks derives from the
8
362 trachyte waste; its abundance gradually decreases with increasing firing temperature (Table 3).

11
1363

14 364 **4.2.2 Radionuclides activity concentration**

16
1365 The radioactivity levels measured in the studied bricks are comparable with those reported in the
18
19
366 literature [5,7,13,52,53,54]. The lowest ^{226}Ra value was measured in brick N, equal to 29 Bq/kg
20
21
367 (Table 4). This value is lower than that measured in the clay GP used to produce this brick (45 Bq/kg).

23
24
368 This can be explained assuming a dilution effect due to the addition of the dye additive MN, which
25
26
369 presents the lowest concentration of natural nuclide among the studied materials (Table 4). The same
27
28
370 effect can be invoked when the sludge F (Table 4) is added to the same clayey material LG.

30
31
371 Radionuclide concentration in the brick FM results to be lower (40 Bq/kg) than that of the brick
32
33
372 obtained using the same clay but tempered with standard quartz-rich sand SS (brick GP, 45 Bq/kg).

35
36
373 Conversely, the brick B_PIR, obtained from the same clay LG with the addition of the sludge PIR,
37
38
374 characterised by a high radioactive concentration (120 Bq/kg), displays higher ^{226}Ra concentration
40
41
375 (55 Bq/kg) than brick GP (Table 4). The same considerations apply to ^{232}Th and ^{40}K concentrations.

42
43
376 Bricks tempered with the trachyte waste TR present generally higher radioactive concentration than
44
45
46
377 the corresponding commercial bricks obtained using the same clay tempered with a quartz-rich sand
47
48
378 (brick RCF, 43 Bq/kg). Bricks tempered with trachyte waste have values of ^{226}Ra concentration
49

50
51
379 between 46 and 55 Bq/kg, while ^{232}Th concentration ranges between 43 and 56 Bq/kg, except for
52
53
380 bricks B5.9 and B15.11, in which it is 66 Bq/kg. ^{40}K concentration for this set of bricks is comprised
54
55
381 between ~ 600 and 1016 Bq/kg, and the maximum values have been measured for bricks B5.9 (1016
56
382 Bq/kg), B5.11 and B15.11 (1000 Bq/kg).

59
60
61
62
63
64
65

383 The activity indexes (Table 4) range between 0.53 and 0.82 for I and 0.15 and 0.27 for I α ,
1
384 respectively. None of the two parameters exceeds the reference levels reported in the Council
3
4
385 Directive 2013/59/Euratom [34] and RP112 [12]. The radium equivalent activity (Ra_{eq}) is always
6
386 < 370 Bq/kg.

387

388 **4.2.3 Radon exhalation rate**

389 In order to determine the contribution of the by-products to the internal radiation dose, which accounts
14
15
390 for the largest fraction of radiation dose from building materials, ²²²Rn emission of the investigated
18
19
391 bricks was measured. Table 5 lists the radon exhalation rates and emanation fraction. Among the
20
21
392 commercial bricks analysed, the lowest radon exhalation rate has been recorded for brick RCF (Table
23
24
393 5), produced using the clay material (LRSSF) with the lowest carbonate content (see CaO wt. % in
25
26
394 Table 2). The bricks produced with clays richer in carbonates show wide variability. All the bricks
28
29
395 produced with the clay LG, enriched in carbonates, and tempered with different materials (bricks GP,
30
31
396 N, FM and B_PIR) show considerable differences in their exhalation rate. This is undoubtedly
33
34
397 partially determined by differences in the chemical composition of the temper (e.g. bricks FM and
35
36
398 B_PIR made using the two different types of ceramic sludge), partially by the textural features,
37
38
399 especially porosity, which develops during firing upon CO₂ release from calcinated carbonates, and
40
41
400 depending on the different reactions taking place at increasing temperature and on the specific temper
42
43
401 used. This is particularly evident when considering the two bricks RSS and R6, both based on clay
44
45
402 LRSS and the same quartz-rich temper but displaying significantly different ²²²Rn exhalation rate
47
48
403 (0.017 Bq/d and 0.084 Bq/d, respectively). In these two materials, the different firing temperatures
49
50
404 (950 °C for RSS vs. 600 °C for R6) determined the development of significantly different textures,
52
53
405 in terms of both pore-size distribution and pore fraction [35]. Since ²²⁶Ra, the precursor of ²²²Rn, has
54
55
406 the same concentration in both bricks (Table 4), the high radon exhalation rate observed in brick R6
57
58
407 (Table 5), is reasonably determined by the different pore structure. The same stands for the lower

59
60
61
62
63
64
65

408 surface exhalation rate of brick RSS ($2.84 \text{ Bq/d}\cdot\text{m}^2$) as compared to brick R6 ($8.58 \text{ Bq/d}\cdot\text{m}^2$) (Table
1
409 5).

410 Bricks obtained using trachyte waste as a temper have generally higher exhalation rate when fired at
4
5
6
7
8
9
10
412 lower temperature (e.g. $900 \text{ }^\circ\text{C}$). Moreover, radon exhalation rate decreases increasing the amount of
11
12
13
14
15
414 trachyte waste added (Table 5). This is apparently a contradiction, considering that trachyte has
16
17
18
19
20
416 significantly higher NORM level than clay (Table 4). However, this could be attributed to the
21
22
23
24
25
26
27
28
29
30
31
32
33
34
35
36
37
38
39
40
41
42
43
44
45
46
47
48
49
50
51
52
53
54
55
56
57
58
59
60
61
62
63
64
65

417 Bricks produced with addition of sludge (FM and B_PIR) have intermediate values of surface
23
24
25
26
27
28
29
30
31
32
33
34
35
36
37
38
39
40
41
42
43
44
45
46
47
48
49
50
51
52
53
54
55
56
57
58
59
60
61
62
63
64
65

4.2.4 Density and porosity

421 Bricks (GP, N, FM, B_PIR and RS) obtained using a carbonate-rich clay (LG and LRS) yielded the
31
32
33
34
35
36
37
38
39
40
41
42
43
44
45
46
47
48
49
50
51
52
53
54
55
56
57
58
59
60
61
62
63
64
65

433 Commercial bricks (RSS, R6 and RCF) produced using carbonate-poor clays (LRSS and LRSSF)
1
434 display lower open porosity (between 34% and 39%, Table 6), with brick R6 showing the lowest
3
435 value, being fired at low temperature (600 °C). This brick has an apparent density ($\rho_a = 1700 \text{ kg/m}^3$)
6
436 considerably different from the actual density ($\rho_r = 2580 \text{ kg/m}^3$), suggesting a high fraction of closed
8
437 pores. Nevertheless, small size open pores remain predominant, as confirmed by the high value of
10
438 adsorbed nitrogen leading to a specific area of $10.24 \text{ m}^2/\text{g}$ according to the BET method, i.e. the
13
439 highest micro-porosity value among all the other samples (Table 6).

440 Open porosity in bricks obtained by adding trachyte waste is quite variable but shows a general trend:
18
441 it increases in bricks fired at 1000 °C and decreases in those fired at 1100 °C, while bulk density (ρ_r)
20
442 increases with the firing temperature. Evaluating the pore range $< 0.1 \text{ }\mu\text{m}$, small pores prevail in
23
443 bricks fired at 900 °C; their fraction gradually decreases with increasing firing temperature and with
25
444 increasing trachyte waste content, also when compared with brick RCF obtained using the same clay,
28
445 but different temper. Thus, the addition of trachyte tailings in the experimental bricks is likely
30
446 responsible of changes in the microstructure, enhancing bulk density and pore size, leading to the
32
447 formation of a more compact material [30]. Changes in the pore system are also well demonstrated
35
448 by the decrease of the specific surface area at increasing firing temperature, as confirmed by the BET
37
449 experiment (Table 6).

451 5. Discussion

452 The obtained emanation coefficients range between 0.002 and 0.109 (Table 5) in agreement with
47
453 those reported by Stoulos et al. (2003) [13] and Righi and Bruzzi (2006) [44]. Most of the bricks have
49
50
454 η value below 0.04, with the exception of brick R6 reaching 0.109; this result is related to the material
52
455 texture and porosity [4,56,57,58], despite the radionuclide concentration being similar to that
54
55
456 observed for the other bricks (Table 4).

58
457 The main parameters describing radon release from a solid are the radon surface exhalation rate Ea
59
60
458 ($\text{Bq/d}\cdot\text{m}^2$), and the radon mass exhalation rate Em ($\text{Bq/d}\cdot\text{kg}$). These values can be either obtained
61
62
63
64
65

459 from direct measurements [56] or estimated when other parameters of the materials are known
 1
 460 [58,59], i.e. the ^{226}Ra activity concentration (C_{Ra} , Bq/kg), the coefficient of emanation (η), the
 3
 461 porosity (ε , %) and the density (ρ , kg/m³). Nonetheless, there are limitations in both these approaches.
 6
 462 Previous works describe porosity as a key factor controlling emanation power of building materials
 8
 463 [13,56], but without quantifying its actual effect. Indeed, porosity plays an important role in physical-
 10
 464 mechanical properties and in the decay behaviour of building materials [27,60,61,62], and so it does
 13
 465 for radon migration [63,64]. Moreover, chemical and mineralogical composition and texture of bricks
 15
 466 may change considerably, depending on the starting raw materials, their relative abundance and grain-
 18
 467 size, and firing conditions [27,35]. Therefore, they represent ideal model materials wherein to
 20
 468 investigate the influence of porosity on radon exhalation. In general, assessment of radon emanation
 23
 469 power requires better understanding on the influence of porosity and pore-size distribution, and on
 25
 470 the influence of radionuclides concentration in relation to texture, which determines the emanation
 28
 471 pathways ultimately determining the effective amount of radon emitted.
 30
 472 Semkow and Parekh (1990) [65] described the importance of grain-size, which controls radon
 33
 473 diffusion through porosity and surface area [66].

474 Mass emanation (Em) normalised to porosity (Em_ε) can be obtained by the following equation:

$$475 \quad Em_\varepsilon = 1 - Em (\varepsilon - C_{\text{Ra}}) / C_{\text{Ra}}$$

476 and mass emanation normalised to ^{226}Ra concentration ($Em_{C_{\text{Ra}}}$) as:

$$477 \quad Em_{C_{\text{Ra}}} = 1 - Em (C_{\text{Ra}} - \varepsilon) / \varepsilon,$$

478 where Em is the measured mass exhalation rate (Bq/d kg), C_{Ra} the ^{226}Ra activity concentration
 47
 479 (Bq/kg), and ε the porosity (%).

50
 5480 The binary plot of radon exhalation rate vs. normalised mass emanation clearly shows a better
 52
 5481 correlation when data are normalised to porosity (Em_ε ; $R^2 = 0.96$; Fig. 2a) than to ^{226}Ra concentration
 54
 5482 ($Em_{C_{\text{Ra}}}$; $R^2 = 0.86$; Fig. 2b). This suggests that texture, and especially open porosity, affects radon
 57
 5483 exhalation more than ^{226}Ra concentration.
 59
 60
 61
 62
 63
 64
 65

484 According to Semkow and Parekh (1990) [65], radon emanation power is sensitive to pores with size
1
2
3
4
5
6
7
8
9
10
11
12
13
14
15
16
17
18
19
20
21
22
23
24
25
26
27
28
29
30
31
32
33
34
35
36
37
38
39
40
41
42
43
44
45
46
47
48
49
50
51
52
53
54
55
56
57
58
59
60
61
62
63
64
65

485 between $5 \cdot 10^{-40}$ μm and $0.1 \mu\text{m}$, although the latter are a key for radon transport inside the material.

486 This is confirmed by the data collected on bricks in the present study. The correlation between
487 emanation mass (Em) measured by E-PERM and total porosity as measured by MIP (Fig. 3a) is very
488 poor ($R^2 = 0.03$), while the one with the fraction of pores $< 0.1 \mu\text{m}$ (Fig. 3b) is considerably better
489 ($R^2 = 0.59$). This suggests that the fraction of smaller pores is the most reactive to radon emission.

490 The same behaviour is observed considering the specific surface areas, S_0 . The specific surface area
491 can be calculated from the average pore radius r (assuming all pores are cylindrical) [35,67], and the
492 total pore intrusion volume dV/V (measured by MIP) as follows:

$$493 S_0 = 2\pi r h$$

494 where the average height (h) is calculate as:

$$495 h = \frac{dV^2}{V} / \pi r$$

496 The correlation between radon emanation mass and specific surface area (m^2/g) is much higher ($R^2 =$
497 0.60 ; Fig. 3c) than considering the total porosity (Fig. 3a). This is related to a linear relationship
498 between emanation power and the specific surface area [68]. This observation is supported also by
499 the data obtained from BET, wherein pores with diameter below $0.3 \mu\text{m}$ are analysed, although radon
500 mass emanation and BET surface areas correlation is not so straightforward ($R^2 = 0.48$; Fig. 3d).

501 A similar result was obtained comparing radon emanation mass with the specific surface area S_0
502 assuming the average pore size equal to $0.005 \mu\text{m}$ and determining h by partial dV/V calculated in
503 the range of pores less than $0.005 \mu\text{m}$: R^2 value obtained in such condition (0.39 , Fig. 3e), is similar
504 to what obtained by BET (0.48 , Fig. 3d). Thus, despite different analytical methods for the
505 determination of the pores system are considered, the specific surface area is in such case related to
506 a range of pores size overlapping in MIP and BET. According to Semkow and Parekh (1990) [65],
507 the emanation power is less sensitive to larger pores. This is also observed for the studied bricks;
508 when the specific surface area is calculated over the total porosity using an average pore size of 0.5
509 μm (Fig. 3f), the parameters are not correlated ($R^2 = 0.04$).

Principal Component Analysis (PCA) (Fig. 4a) applied to the main physical properties and chemical components of the bricks further indicates the correlations among textural features, chemistry and radioactivity. The purpose of this analysis is to determine which of these variables is mostly affecting radon emanation of the bricks. The score and loading plot of the first three components (Fig. 4a), shows that PC1 is positively correlated with MnO, CaO and MgO that are grouped with BET surface area (S_{aBET}), while it is negatively correlated with variables associated with natural radionuclides activity concentration, bulk density and Fe-oxides. PC2 is positively correlated with variables related to radon exhalation (Ea and Em), LOI, and fine-size porosity (BET surface area S_{aBET} and $\epsilon_{MIP<0.1\mu m}$). In order to enlighten differences among the various bricks, the binary plot of PC1 and PC2 was also considered (Fig. 4b). In this case bricks are distributed according to their specific mix design. Thus, bricks obtained from the most siliceous clay (LRSSF) with the addition of trachyte waste are all clustered together as a result of the highest radioactive content, expressed by the values of I , $I\alpha$ and C_{Ra} , the highest bulk density and content of Al_2O_3 , Na_2O , TiO_2 , P_2O_3 , Ni , and Rb . On the other hand, bricks obtained from the carbonate-rich clay (LG) are grouped in correspondence to CaO and MgO. Therefore, PCA summarizes the influence of different mineralogical, chemical and physical variables in relation with radon emanation and transport.

6. Conclusions

Radioactivity and radon exhalation rate of bricks produced using NORM by-products have been determined and compared with those of similar commercial bricks. All investigated samples provided values below the reference levels indicated in the Council Directive 2013/59/Euratom concerning basic safety standards for protection against exposure to ionising radiations.

While radon emanation in bricks is primarily determined by the concentration of the parent radionuclides from the uranium-238 series in the samples resulting from the composition of the mixture of natural and waste materials, radon exhalation also depends on the pore system, which controls radon mobility. Because the characteristics of the pore system are influenced by the initial

536 mineral composition and by the transformations taking place during firing process, firing conditions
1
537 also contribute to determine net radon exhalation rate. Starting from the same clayey material as
3
538 commercial brick RCF and adding increasing proportions of trachyte waste, we may expect a
6
539 progressive increase of radon exhalation. Instead, although all the samples produced adding the
8
540 trachyte waste present higher exhalation rate compared to brick RCF, our data show that radon
10
541 exhalation rate decreases by increasing the amount of trachyte. This can be explained by considering
13
542 that the alkali feldspar present in the trachyte waste acts as a flux, thus promoting sintering
15
543 proportional with trachyte waste content and firing temperature. Total open porosity initially
18
544 increases from 900 °C to 1000 °C due to proceeding of sheet silicates decomposition, and then
20
545 decreases from 1000 °C to 1100 °C, due to further sintering, while open porosity < 0.1 µm and surface
23
546 area (both BET and MIP) continuously decrease with increasing temperature. A similar observation
25
547 arises considering samples RSS and R6. These two samples have the same composition, but they
28
548 have been fired at different temperatures (950 °C and 600 °C, respectively). For this reason they have
30
549 similar ²²⁶Ra, ²³²Th and ⁴⁰K radioactivity concentration, but significantly different radon exhalation
32
550 rate, which is four times lower in the sample RSS fired at higher temperature. In this sample,
35
551 carbonate decomposition and consequent fluxing effect of the released CaO determined an increase
37
552 in total open porosity, but a significant reduction of open porosity < 0.1 µm and surface area (both
40
553 BET and MIP), similarly to what observed in samples containing trachyte waste.
42
554 This indicates that texture evolution during firing determines significant changes in porosity and pore
45
555 size distribution, eventually determining changes in gas transport pathways through the pore system
47
556 and modifying radon exhalation rate.
49

50
557

558 **Acknowledgments**

559 This study was funded by Project CPDA134483 of the University of Padova (Raffaele Sassi) and by
57
560 Junta de Andalucía Research Group RNM179 and by Research Project MAT2016-75889-R
59
60
61
62
63
64
65

561 (Giuseppe Cultrone). The authors are grateful to the company *SanMarcoTerreal Italia srl* for
1
562 collaborating in providing materials and supporting technologies.

563

564 **References**

565 [1] M. Al-Jarallah, Radon exhalation from granites used in Saudi Arabia, *J. Environ. Radioact.*
10
11 53 (2001) 91–98.

567 [2] R. Hewamanna, C.S. Sumithrarachchi, P. Mahawatte, H.C.L. Nanayakkara, H.C. Ratnayake,
14
15
16 Natural radioactivity and gamma dose from Sri Lankan clay bricks used in building construction,
17
18
19 *Appl. Radiat. Isot.* 54 (2001) 365–369.

570 [3] O. Brígido Flores, A. Montalván Estrada, R. Rosa Suárez, J. Tomás Zerquera, A. Hernández
22
23
24
25 Pérez, Natural radionuclide content in building materials and gamma dose rate in dwellings in
26
27 Cuba, *J. Environ. Radioact.* 99 (2008) 1834–1837.

573 [4] J. Chen, N.M. Rahaman, I.A. Atiya, Radon exhalation from building materials for decorative
30
31
32 use, *J. Environ. Radioact.* 101 (2010) 317–322.

575 [5] N. Damla, U. Cevik, A.I. Kobya, A. Celik, N. Celik, I. Yıldırım, Assessment of natural
35
36
37 radioactivity and mass attenuation coefficients of bricks and roofing tile used in Turkey, *Radiat.*
38
39 *Meas.* 46 (2011). 701–708.

578 [6] H. Kayakökü, Ş. Karatepe, D. Mahmut, Measurements of radioactivity and dose assessments
42
43
44 in some building materials in Bitlis, Turkey, *Appl. Radiat. Isot.* 115 (2016) 172–179.

580 [7] M. Hegedús, Z. Sas, E. Tóth-Bodrogi, T. Szántó, J. Somlai, T. Kovács, Radiological
47
48
49 characterization of clay mixed red mud in particular as regards its leaching features, *J. Environ.*
50
51
52 *Radioact.* 162–163 (2016) 1–7.

583 [8] Y. Raghu, R. Ravisankar, A. Chandrasekaran, P. Vijiayagopal, B. Venkatraman, Assessment
54
55
56
57 of natural radioactivity and radiological hazards in building materials used in the Tiruvannamalai
58
59
60
61
62
63
64
65 Distric, Tamilnadu, India, using a statistical approach, *J. Taibah Univ. Sci.* 11 (2017) 523–533.

- 586 [9] H. Bártová, J. Kucěra, L. Musílek, T. Trojeck, E. Gregorová, Determination of U, Th and K,
1
587 in bricks by gamma-ray spectrometry, X-ray fluorescence analysis and neutron activation
3
4
588 analysis, *Radiat. Phys. Chem.* 140 (2017) 161–166.
5
6
589 [10] D. Langimur, Uranium-solution equilibria at low temperatures with applications to
8
9
590 sedimentary Ore deposits, *Geochim. Cosmochim. Acta* 42 (6) (1978) 547–569.
10
11
591 [11] O. Maxwell, H. Wagiran, N. Ibrahim, S.K. Lee, Z. Embong, P.E. Ugwuoke, Natural
13
14
592 radioactivity and geological influence on subsurface layers at Kubwa and Gosa area of Abuja,
15
16
593 Northcentral Nigeria, *J. Radional. Nucl. Ch.* 303 (2015) 821–830.
18
19
594 [12] European Commission (1999). Radiation Protection 112, Radiological protection principles
20
21
595 concerning the natural radioactivity of building materials, Directorate-General Environment,
23
24
596 Nuclear Safety and Civil Protection, Luxembourg ISBN 92-828-8376-0.
25
26
597 [13] S. Stoulos, M. Manolopoulou, C. Papastefanou, Assessment of natural radiation exposure
27
28
598 and radon exhalation from building materials in Greece, *J. Environ. Radioact.* 69 (2003) 225–240
30
31
599 [14] H. Friedmann, C. Nuccetelli, B. Michalik, M. Anagnostakis, G. Xhixha, K. Kovler, G. de
32
33
600 With, C. Gascó, W. Schroeyers, R. Trevisi, S. Antropov, A. Tsapalov, C. Kunze, N.P,
35
36
601 Petropoulos, Measurement in NORM, Naturally occurring Radioactive Materials in Construction,
37
38
602 Integrating Radiation Protection in Reuse, (COST Action Tu1301 Norm4building), Edit by
40
41
603 Wouter Schroeyers, Woodhead Publishing (2017) 61–134.
42
43
604 [15] K. Kovler, The national survey of natural radioactivity in concrete produced in Israel, *J.*
44
45
605 *Environ. Radioact.* 168 (2017) 46–53.
47
48
606 [16] M.P. Campos, L.J.P. Costa, M.B. Nisti, B.P. Mazzilli, Phosphogypsum recycling in the
49
50
607 building materials industry: assessment of the radon exhalation rate, *J. Environ. Radioact.* 172
52
53
608 (2017) 232–236.
54
55
609 [17] M. Rafique, S.U. Rahman, T. Mahmood, S. Rahman, Matiullah S.U., Rehman Radon
57
58
610 exhalation rate from soil, sand, bricks, and sedimentary samples collected from Azad Kashmir,
59
60
611 Pakistan, *Russ. Geol. Geophys.* 52 (2011) 450–457.
62
63
64
65

- 612 [18] J. Porstenörfen, Properties and behaviour of Radon and Thoron and their decay products in
1 the air, *J. Aerosol Sc.* 25, 2 (1994) 219–263.
- 613
3
4
614 [19] World Health Organization. WHO Report on the Global Tobacco Epidemic-The MPOWER
5
6
615 package. WHO; Geneva (2008).
- 616 [20] M. Dondi, M. Marsigli, B. Fabbri, Recycling of industrial and urban wastes in brick
7
8
9
10
11
12
13
14
618 [21] M. Dondi, M. Marsigli, B. Fabbri, Recycling of industrial and urban wastes in brick
15
16
17
18
19
620 [22] P. Duminuco, B. Messiga, M.P. Riccardi, Firing process of natural clays. Some microtextures
20
21
22
23
24
25
26
623 [23] M.P. Riccardi, B. Messiga, P. Duminuco, An approach to the dynamics of clay firing, *Appl.*
27
28
29
30
31
625 [24] G. Cultrone, E. Sebastián, Fly ash addition in clayey materials to improve the quality of solid
32
33
34
35
36
627 [25] L. Zhang, Production of bricks from waste materials – A review, *Constr. Build. Mater.* 47
37
38
39
40
41
42
43
630 [26] P. Muñoz Velasco, M.P. Morales Ortíz, M.A. Mendivil Giró, L. Muñoz Velasco Fired clay
44
45
46
47
48
49
50
51
52
53
634 [27] C. Coletti, G. Cultrone, L. Maritan, C. Mazzoli, How to face the new industrial challenge of
54
55
56
57
58
636 [28] S.M. Saleem Kazmi, M.J. Munir, Y.F. Wu, A. Hanif, I. Patnaikuni, Thermal performance
59
60
61
62
63
64
65

- 637 [29] E. Franzoni, Materials selection for green buildings: which tools for engineers and
1 architects?, *Procedia Eng.* 21 (2011) 883–890.
- 638
3
4
639 [30] C. Coletti, L. Maritan, G. Cultrone, A. Hein, M.C. Dalconi, E. Molina C. Mazzoli, Recycling
6 trachyte waste from quarry to brick industry: effects on petrophysical properties and durability of
640 new bricks, *Constr. Build. Mater.* 166 (2018) 792–807.
- 641
10
11
642 [31] R.M. Amin, A study of radon emitted from building materials using solid state nuclear track
13 detectors, *J. Radiat. Res. Appl. Sci.* 8 (2015) 516–522.
- 643
14
15
16
644 [32] C. Coletti, G. Cultrone, L. Maritan, C. Mazzoli, Combined multi-analytical approach for
18 study of pore system in bricks: How much porosity is there?, *Mater. Charact.* 121 (2016) 82–92.
- 645
19
20
21
646 [33] J. Labrincha, F. Pueras, W. Schroeyers, K. Kovler, Y. Pontikes, C. Nuccetelli, P. Krivenko,
23 O. Kovalchuk, O. Petropavlovsky, M. Komljenovic, E. Fidanchevchki, R. Wieggers, E.
647 Volceanov, E. Gunay, M.A. Sanjuán, V. Ducman, B. Angjusheva, D. Bajare, T. Kovacs, G. Bator,
25 S. Schreurs, J. Aguiar, J.L. Provis, From NORM by-products to building materials, *Naturally
26 Occurring Radioactive Materials in Construction, Integrating Radiation Protection in Reuse,
648 (COST Action Tu1301 Norm4building)*, Edit by Wouter Schroeyers, Woodhead Publishing
27 (2017) 183–252.
- 649
30
31
650 [34] European Union (2013). Council Directive 2013/59/Euratom of 5 December 2013 laying
32 down basic safety standards for protection against the dangers arising from exposure to ionising
33 radiation, and repealing Directives 89/618/Euratom, 90/641/Euratom, 96/29/Euratom, 97/43/
651 Euratom and 2003/122/Euratom. *Official Journal of the European Union*, OJ L13, 17.01.2014,
35 pp. 1–73.
- 652
36
37
38
653 [35] C. Coletti, L. Maritan, G. Cultrone, C. Mazzoli, Use of industrial ceramic sludge in brick
39 production: Effect on aesthetic quality and physical properties, *Constr. Build. Mater.* 124 (2016)
40 219–227.
- 654
41
42
43
655
44
45
656
46
47
657
48
49
50
658
51
52
659
53
54
55
660
56
57
58
59
60
61
62
63
64
65

- 661 [36] M.F. Attallah, M.A. Hilal, S.I. Moussa, Quantification of some elements of nuclear and
1 industrial interest from zircon mineral using neutron activation analysis and passive gamma-ray
662 Spectroscopy, *Appl. Radiat. Isotopes* 128 (2017) 224–230.
3
4
663 [37] L. Tositti, G. Cinelli, E. Brattich, A. Galgaro, D. Mostacci, C. Mazzoli, M. Massironi, R.
6
664 Sassi, Assessment of lithogenic radioactivity in the Euganean Hills magmatic district (NE Italy),
8
665 *J. Environ. Radioact.* 166 (2017) 259–269..
10
11
666 [38] V.D. Scott, G. Love, *Quantitative Electron Probe Microanalysis*. John Wiley and Sons, New
13
667 York (1983).
14
15
668 [39] G. Chen, J. Wang, The preparation of marine geological certified reference materials -
16
669 polymetallic nodule GSPN-1 and marine sediment GSMS-1 from the Central Pacific Ocean,
18
670 *Geostand. Geoanal. Res.* 22 (1998) 119–125.
20
21
671 [40] G. Cinelli, L. Tositti, B. Capaccioni, E. Brattich, D. Mostacci, Soil gas radon assessment and
23
672 development of a radon risk map in Bolena, Central Italy, *Environ. Geochem. Health* 37 (2014)
25
673 305–319.
26
674 [41] G. Gilmore, “*Practical gamma-ray Spectroscopy*” 2nd edition, Wiley (2008).
28
675 [42] D.C. Stromswold, Calibration facilities for borehole and surface environmental radiation
30
676 measurements, *J. Radioanal. Nucl. Ch.* 194 (1995) 393–401.
31
677 [43] Nordic, 2000. Naturally occurring Radiation in Nordic Countries—Recommendation. In:
33
678 The Flag-Book series, The Radiation Protection Authorities in Denmark, Finland, Norway and
35
679 Sweden, Reykjavik.
36
680 [44] S. Righi, L. Bruzzi, Natural radioactivity and radon exhalation in building materials used in
38
681 Italian dwellings, *J. Environ. Radioact.* 88 (2006) 158–170.
39
682 [45] J. Beretka, P.J. Matthew, Natural radioactivity of Australian building materials, industrial
40
683 wastes and by-products, *Health Phys.* 48 (1985) 87–95.
41
684
42
43
44
45
46
47
48
49
50
51
52
53
54
55
56
57
58
59
60
61
62
63
64
65

- 685 [46] L. Germinario, J.H. Hanchar, R. Sassi, L. Maritan, R. Cossio, A. Borghi, C. Mazzoli, New
1 petrographic and geochemical tracers for recognizing the provenance quarry of trachyte of the
686 Euganean Hills, northeastern Italy, *Geoarchaeology* 33 (2018) 430–452.
3
4
687
6
688 [47] G. Cultrone, E. Sebastián, K. Elert, M.J. de la Torre, O. Cazalla, C. Rodriguez-Navarro,
8
9
689 Influence of mineralogy and firing temperature in the porosity of bricks, *J. Eur. Ceram. Soc.* 34
10
11
690 (2004) 547–564.
13
14
691 [48] L. Damonte, P. Rivas, A. Pasquevich, F. Andreola, F. Bondioli, A. M. Ferrari, L. Tositti, G.
15
16
692 Cinelli, Structural Characterization of natural and processed zircons with X-rays and nuclear
18
19
693 techniques, *Adv. Condens. Matter Phys.* (2017) 1–9.
20
21
694 [49] A. Sakoda, Y. Nishiyama, K. Hanamoto, Y. Ishimori, Y. Yamamoto, T. Kataoka, A. Kawabe,
23
24
695 K. Yamaoka, Differences of natural radioactivity and radon emanation fraction among constituent
25
26
696 minerals of rock or soil, *Appl. Radiat. Isotopes* 68 (2010) 1180–1184.
27
28
697 [50] G. Cultrone, C. Rodriguez-Navarro, E.M. Sebastián, O. Cazalla, M.J. de la Torre, Carbonate
30
31
698 and silicate phase reactions during ceramic firing, *Eur. J. Mineral.* 13 (2001) 621–634.
32
33
699 [51] L. Maritan, L. Nodari, C. Mazzoli, A. Milano, U. Russo, Influence of firing conditions in
35
36
700 ceramic products: experimental study on clay rich in organic matter, *Appl. Clay Sci.* 31 (2006)
37
38
701 1–15.
40
41
702 [52] R. Trevisi, S. Risica, M. D’Alessandro, D. Paradiso, C. Nuccetelli, Natural radioactivity in
42
43
703 building materials in the European Union: a database and an estimate of radiological significance,
44
45
704 *J. Environ. Radioact.* 105 (2012) 11–20.
47
48
705 [53] G. De With, P. de Jong, A. Röttger, Measurement of thoron exhalation rate from building
49
50
706 materials, *Health Phys.* 7, Volume 107, Number 3 (2014) 206–212.
52
53
707 [54] R. Trevisi, F. Leonardi, S. Risica, C. Nuccetelli, Updated database on natural radioactivity
54
55
708 in building materials in Europe, *J. Environ. Radioact.* 187 (2018) 90–105.
57
58
709 [55] Z. Sas, J. Somlai, G. Szeiler, T. Kovács, Radon emanation and exhalation characteristics of
59
60
710 heat-treated clay samples, *Radiat. Prot. Dosim.* 152 (2012) 51–54.
62
63
64
65

- 711 [56] M. Marocchi, S. Righi, G.M. Bargossi, G. Gasparotto, Natural radionuclides content and
1 radiological hazard of commercial ornamental stones: an integrated radiometric and
212 2 mineralogical-petrographic study, *Radiat. Meas.* 46 (2011) 538–545.
3
4
513
6
714 [57] T. Kovacs, G. Bator, W. Schroeyers, J. Labrincha, F. Puertas, M. Hegedus, D. Nicolaidis,
8
9
1015 M.A. Sanjuán, P. Krivenko, I.N. Grubeša, Z. Sas, B. Michalik, M. Anagnostakis, I. Barisic, C.
11
1216 Nuccetelli, R. Trevisi, T. Croymans, S. Schreurs, N. Todorović, D. Vaiciukyniene, R. Bistrickaite,
13
14
1517 A. Tkaczyk, K. Kovler, R. Wiegers, R. Doherty, From raw materials to NORM by-products,
16
1718 *Naturally Occurring Radioactive Materials in Construction* (2017) 135–182.
18
1919 [58] Z. Sas, N. Vandevenne Rory Doherty, R. Vinai, J. Kwasny, M. Russell, W. Sha, M. Soutsos,
20
21
2220 W. Schroeyers, Radiological evaluation of industrial residues for construction purposes correlated
23
2421 with their chemical properties, *Sci. Total Environ.* 658 (2019) 141–151.
25
26
2722 [59] W.W. Nazaroff, A.V. Nero Jr., *Radon and Its Decay Products in Indoor Air*. Wiley, New
28
2923 York (1988).
30
31
32724 [60] L. Germinario, G.F. Andriani, R. Laviano, Decay of calcareous building stone under the
33
3425 combined action of thermoclastism and cryoclastism: A laboratory simulation, *Constr. Build.*
35
3626 *Mater.* 75 (2015) 385–394.
37
38
3927 [61] C. Di Benedetto, P. Cappelletti, M. Favaro, S.F. Graziano, A. Langella, D. Calcaterra, A.
40
4128 Colella Porosity as key factor in the durability of two historical building stones: Neapolitan
42
43
4429 Yellow Tuff and Vicenza Stone, *Eng Geol.* 193 (2015) 310–319.
45
4630 [62] S. Scrivano, L. Gaggero, J.G. Aguilar Micro-porosity and minero-petrographic features
47
48
4931 influences on decay: Experimental data from four dimension stones, *Constr. Build. Mater.* 173
50
5132 (2018) 342–349.
52
53
5433 [63] A.B. Tanner, Radon migration in the ground. In *the Natural Radiation Environment*,
55
5634 Houston, TX (1978).
57
58
59
60
61
62
63
64
65

- 735 [64] N.M. Hassan, M. Hosoda, T. Ishikawa, A. Sorimachi, S.K. Sahoo, S. Tokonami, M. Fukushima,
 1
 736 Radon Migration Process and Its Influence Factors; Review. *Jpn. J. Health Phys.* 44 (2) (2009)
 3
 737 218–231.
 4
 5
 6
 738 [65] T.M. Semkow, P.P. Parekh, The role of radium distribution and porosity in radon emanation
 8
 739 from soils, *Geophys. Res. Lett.* Vol. 17, no. 6, (1990) 837–840.
 9
 10
 11
 1240 [66] S.A. Mujahid, S. Hussain, A.H. Dogar, S. Karim, Determination of porosity of different
 13
 14 materials by radon diffusion, *Radiat. Meas.* 40 (2005) 106–109.
 15
 16
 1742 [67] H. Giesche, Mercury Porosimetry: A General (Practical) Overview. Part. Part. Syst. Charact.
 18
 19 23 (2006) 9–19.
 20
 21
 2244 [68] D.A.W. Bossus, Emanating power and specific surface area, *Radiat. Prot. Dosimetry* v. 7
 23
 24 (1984) 73–76.
 25
 26
 2746 [69] D.L. Whitney, B.W. Evans Abbreviations for names of rock-forming minerals, *Am. Mineral.*
 28
 29 95 (2010) 185–187.
 30
 31
 32

33
 34
 35
 36
 37
 38
 39
 40
 41
 42
 43
 44
 45
 46
 47
 48
 49
 50
 51
 52
 53
 54
 55
 56
 57
 58
 59
 60
 61
 62
 63
 64
 65

Table headings

Table 1: Raw materials (clayey materials, temper and additives) and bricks production recipe (with relative firing temperature).

Table 2: Chemical composition of raw materials and bricks, expressed in wt. % of oxides for the major and minor elements and Loss On Ignition (LOI), and trace elements expressed in ppm. < DL: below the detection limit. *: not measured.

Table 3: Mineralogical composition of clayey materials, temper, additive and bricks determined by XRPD. Mineral abbreviations after Whitney and Evans (2010) [69]: Qz = quartz; Pl = plagioclase; Afs = alkali-feldspar; Cal = calcite; Dol = dolomite; Ill = illite; Chl = chlorite; Bt = Biotite; Hem = hematite; Hsm = hausmannite; Crs = Cristobalite; Mul = mullite; Di = diopside; Gh = gehlenite;

761 Wo = wollastonite; Bst = bustamite; Kln = kaolinite; Crd = cordierite; AM = amorphous. Estimated
1
762 relative abundance: ***** = very abundant; *** = abundant; ** = medium; * = scarce; + = rare; - =
3
4
763 absent.
5
6

764
8
9
765 **Table 4:** Natural radioactivity in raw materials and bricks including activity concentrations of ^{226}Ra ,
10
11
1266 ^{232}Th , and ^{40}K (Bq/kg) , concentration of elemental U, Th, and K (ppm) and I_{α} and I indexes and
13
14
767 Ra_{eq} (Bq/kg). Experimental data below the Minimum Detectable Activity (MDA) are reported as
15
16
768 <MDA as determined from spectrum processing.
18

19
769
20
21
2270 **Table 5:** E-PERM results: Q_A , exhalation rate (Bq/d); E_a , surface exhalation rate (Bq/d·m²); E_m ,
23
2471 mass exhalation rate (Bq/d·kg); η , emanation coefficient.
25

26
2772
28
2973 **Table 6:** Physical parameters. MIP results: ϵ_{tot} , total open porosity (%); ρ_r , bulk/real density (kg/m);
30
31
774 ρ_a , apparent density (kg/m); $\epsilon_{<0.1\mu m}$, open porosity < 0.1 μm (%); $\epsilon_{<1\mu m}$, open porosity < 1 μm (%);
32
33
775 $\epsilon_{>1\mu m}$, open porosity > 1 μm (%); $\epsilon_{0.1-1\mu m}$, open porosity between 0.1 and 1 μm (%). N₂ adsorption:
35
36
776 S_{aBET} , BET surface area (m²/g). MIP: S_{aMIP} , MIP surface area (m²/g); $S_{aMIP<0.05\mu m}$, surface area for
37
38
777 pores < 0.05 μm (m²/g); $S_{aMIP<0.5\mu m}$, surface area for pores < 0.5 μm (m²/g).
40

41 42 43 4479 **List of Figures**

45
4680 **Figure 1:** a) Dendrogram of cluster analysis according to average linkage method and square
47
48
781 Euclidean distance; b) score and loading plot of the principal component analysis performed on the
49
50
5182 XRF chemical data of the studied bricks. PC1, PC2 and PC3 cover 41.3%, 30.8% and 12.2% (total
52
53
783 84.3%) of the total variance, respectively.
54
55

5684

57
58
59
60
61
62
63
64
65

785 **Figure 2:** Correlation between radon mass exhalation rate (Em) versus: a) mass emission (Em_ϵ)
1
786 normalised for total porosity considering all the studied bricks; b) mass emission (Em_{CRa}) normalised
3
787 for ^{226}Ra concentration considering all the studied bricks.
4
5
6

788
8
9
789 **Figure 3:** a) correlation between measured radon mass exhalation rate Em (Bq/d·kg) and total
10 porosity ϵ (%); b) correlation between measured radon mass exhalation rate Em (Bq/d·kg) and open
11 porosity $\epsilon_{<0.1\mu\text{m}}$ (%); c) correlation between measured radon mass exhalation rate Em
12 (Bq/d·kg) and surface area S_{aMIP} , determined by MIP measurements, (m^2/g); d) correlation between
13 measured radon mass exhalation rate Em (Bq/d·kg) and surface area S_{aBET} , determined by BET
14 measurements (m^2/g); e) correlation between measured radon mass exhalation rate Em (Bq/d·kg) and
15 surface area for pores $< 0.05 \mu\text{m}$ $S_{aMIP<0.05\mu\text{m}}$, determined by MIP measurements, (m^2/g); f) correlation
16 between measured radon mass exhalation rate Em (Bq/d·kg) and surface area for pores $< 0.5 \mu\text{m}$
17 $S_{aMIP<0.5\mu\text{m}}$, determined by MIP measurements (m^2/g).
18
19
20
21
22
23
24
25
26
27
28
29
30

31
32
33
34
35
36
37
38
39
40
41
42
43
44
45
46
47
48
49
50

506 **Figure 4:** Scores and loading plots of PCA performed on the following variables: $I\alpha$ index; I index;
507 the major elements SiO_2 , TiO_2 , Al_2O_3 , Fe_2O_3 , CaO , MgO , MnO , Na_2O , K_2O and P_2O_5 (expressed as
508 wt. %); the trace elements Zr, Rb, Sr, Pb, Cr, Ni and Zn (expressed as ppm); LOI (Lost On Ignition,
509 wt. %); ϵ_{tot} , total open porosity (%); ρ_r , real density (kg/m^3); $\epsilon_{<0.1\mu\text{m}}$, open porosity $< 0.1\mu\text{m}$ (%); S_{aBET} ,
510 BET surface area (m^2/g); S_{aMIP} , MIP surface area (m^2/g); Em , radon mass exhalation rate (Bq/d·kg);
511 Ea , radon surface exhalation rate (Bq/ d· m^2); C_{Ra} , activities of ^{226}Ra (Bq/kg) PC1, PC2 and PC3
512 representing 34.7%, 26.9% and 16.4% of total variance, respectively.
513
514
515
516
517
518
519
520
521
522
523
524
525
526
527
528
529
530
531
532
533
534
535
536
537
538
539
540
541
542
543
544
545
546
547
548
549
550
551
552
553
554
555
556
557
558
559
560
561
562
563
564
565

507 **Supplementary material:**

508 **Figure 1S:** XRPD pattern of sample PIR. Mineral abbreviations as in Table 3.
509
510
511
512
513
514
515
516
517
518
519
520
521
522
523
524
525
526
527
528
529
530
531
532
533
534
535
536
537
538
539
540
541
542
543
544
545
546
547
548
549
550
551
552
553
554
555
556
557
558
559
560
561
562
563
564
565

	sample	type	
	LG	Clay	
	LRS	Clay	
	LRSS	Clay	
	LRSSF	Clay	
raw materials	SS	Standard temper (quartz-rich sand)	
	TR	Temper (waste 1 = trachyte by-product from quarry)	
	F	Temper (waste 2 = sludge from ceramic industry)	
	PIR	Temper (waste 3 = sludge from ceramic industry)	
	MN	Dye additive (Mn ₂ O ₃ , hausmannite)	
	brick	mix design	firing T (°C)
commercial bricks	GP	Clay LG + siliceous temper (10 wt. %)	1050
	N	Clay LG + siliceous temper (10 wt. %) + MN (15 wt. %)	1050
	RSS	Clay LRSS + siliceous temper (10 wt. %)	950
	R6	Clay LRSS + siliceous temper (10 wt. %)	600
	RS	Clay LRS + siliceous temper (10 wt. %)	980
	RCF	Clay LRSSF + siliceous temper (10 wt. %)	1050
bricks made with trachyte waste	B5.9	Clay LRSSF + temper TR (5 wt. %)	900
	B5.10	Clay LRSSF + temper TR (5 wt. %)	1000
	B5.11	Clay LRSSF + temper TR (5 wt. %)	1100
	B10.9	Clay LRSSF + temper TR (10 wt. %)	900
	B10.10	Clay LRSSF + temper TR (10 wt. %)	1000
	B10.11	Clay LRSSF + temper TR (10 wt. %)	1100
	B15.9	Clay LRSSF + temper TR (15 wt. %)	900
	B15.10	Clay LRSSF + temper TR (15 wt. %)	1000
	B15.11	Clay LRSSF + temper TR (15 wt. %)	1100
bricks made with ceramic sludge	FM	Clay LG + temper F (10 wt. %)	1050
	B_PIR	Clay LG + temper PIR (10 wt. %)	1050

		SiO ₂	Al ₂ O ₃	Fe ₂ O ₃	MnO	MgO	CaO	Na ₂ O	K ₂ O	TiO ₂	P ₂ O ₅	LOI	Zr	Rb	Sr	Pb	Cr	Ni	Zn
raw materials	LG	39.81	10.63	3.87	0.08	4.75	17.76	0.54	2.37	0.43	0.11	19.65	116	81	157	17	74	46	69
	LRS	51.50	12.72	4.43	0.09	3.41	10.45	0.70	2.74	0.54	0.12	13.29	147	98	116	22	89	42	77
	LRSS	57.77	14.14	4.85	0.10	2.68	6.16	1.09	2.99	0.63	0.13	9.47	167	106	86	27	89	36	85
	LRSSF	63.57	13.62	5.06	0.11	2.29	3.85	0.96	2.61	0.84	0.13	6.94	186	96	87	24	115	45	80
	TR	65.27	16.59	3.26	0.07	0.61	1.74	5.06	5.06	0.65	0.18	0.92	674	114	239	18	<DL	1	83
	F	72.52	18.36	1.20	0.01	0.51	1.00	3.11	2.31	0.71	0.11	0.16	1583	*	*	*	*	*	*
	PIR	65.68	17.83	2.07	0.03	0.65	2.19	3.37	1.85	0.60	0.16	4.35	7157	211	567	77	2201	37	4915
commercial bricks	GP	50.17	13.19	4.80	0.09	5.61	20.39	0.72	2.84	0.49	0.13	1.56	128	100	187	20	83	58	80
	N	42.42	11.67	4.93	12.86	4.93	17.63	0.60	2.66	0.52	0.15	1.63	127	90	162	48	76	56	193
	RSS	63.79	15.28	5.16	0.11	2.87	7.01	0.99	3.20	0.66	0.13	0.78	164	118	105	28	90	41	91
	R6	60.32	14.35	4.85	0.11	2.69	6.22	0.93	3.03	0.64	0.13	6.74	149	105	94	25	93	40	81
	RS	59.46	14.53	4.94	0.09	3.69	11.06	0.89	2.99	0.59	0.13	1.62	143	109	135	25	93	51	87
	RCF	65.29	13.81	5.41	0.10	3.06	6.52	1.52	2.41	0.72	0.15	1.01	201	124	181	38	18	78	117
bricks made with trachyte waste	B5.9	64.06	13.92	5.44	0.12	3.06	6.74	1.86	2.39	0.68	0.17	1.56	258	121	218	36	174	108	108
	B5.10	64.23	14.12	5.50	0.12	3.16	6.73	1.88	2.41	0.69	0.18	0.99	234	121	222	34	256	131	102
	B5.11	64.99	14.05	5.48	0.12	3.13	6.76	1.92	2.42	0.68	0.17	0.28	233	122	215	38	160	110	104
	B10.9	63.89	14.24	5.45	0.11	2.98	6.21	2.07	2.58	0.69	0.18	1.60	265	124	224	32	162	108	289
	B10.10	64.34	14.35	5.43	0.10	2.97	6.27	2.09	2.58	0.69	0.18	0.99	259	125	219	35	165	103	104
	B10.11	64.82	14.47	5.52	0.12	3.03	6.29	2.09	2.62	0.71	0.18	0.15	257	126	223	38	170	110	102
	B15.9	64.55	14.40	5.35	0.12	2.81	5.96	2.27	2.71	0.70	0.18	0.93	282	125	227	34	155	93	104
	B15.10	64.41	14.58	5.35	0.11	2.84	5.99	2.31	2.75	0.72	0.18	0.75	285	125	230	30	157	95	105
	B15.11	65.04	14.55	5.42	0.11	2.89	5.94	2.30	2.72	0.72	0.19	0.13	272	125	223	37	143	95	105
bricks made with ceramic sludge	FM	53.88	13.40	4.18	0.08	5.06	17.85	1.43	2.58	0.53	0.12	0.89	323	122	235	33	111	56	360
	B_PIR	54.64	14.11	3.79	0.26	4.53	16.67	1.79	2.40	0.53	0.13	1.14	2032	132	335	131	462	41	1192

		Qz	Itt	Chl	Afs	Pl	Cal	Dol	Hem	Crs	Hsm	Mul	Kln	Bt	AM	
raw materials	LG	****	**	**	*	*	****	***	+		-	-	-	-	-	
	LRS	****	**	**	*	**	**	**	+		-	-	-	-	-	
	LRSS	****	**	**	**	**	*	*	+		-	-	-	-	-	
	LRSSF	****	**	**	**	**	+	+	+		-	-	-	-	-	
	TR	**	-	-	***	***	-	-	-		-	-	-	*		
	F	****	-	-	-	***	-	-	-	+	-	**	-	-	-	**
	PIR	****	*	-	**	***	*	-	-		-	-	*	-	-	-
	MN	-	-	-	-	-	-	-	-		****	-	-	-	-	-
		Qz	Itt	Chl	Afs	Pl	Cal	Dol	Hem	Wo	Di	Gh	Bst	Crđ	Bt	AM
commercial bricks	GP	****	-	-	**	*	-	-	*	**	***	***	-	-	-	**
	N	****	-	-	**	*	-	-	*	**	***	***	***	-	-	***
	RSS	****	-	-	*	**	-	-	*	*	+	+	-	-	-	-
	R6	****	**	**	*	***	**	**	*	-	-	-	-	-	-	-
	RS	****	-	-	*	**	-	-	*	*	*	*	-	-	-	-
	RCF	****	-	-	*	**	-	-	*	*	*	**	-	-	-	-
bricks made with trachyte waste	B5.09	****	*	-	**	**	+	-	*	-	*	*	-	+	+	**
	B5.10	****	+	-	**	**	+	-	*	-	*	**	-	-	+	**
	B5.11	****	-	-	**	**	-	-	*	-	*	***	-	-	+	***
	B10.09	****	+	-	**	**	+	-	*	-	*	*	-	+	+	*
	B10.10	****	+	-	**	**	+	-	*	-	*	**	-	-	+	*
	B10.11	****	-	-	**	**	-	-	*	-	*	***	-	-	+	***
	B15.09	****	*	-	***	***	+	-	*	-	*	*	-	+	++	*
	B15.10	****	+	-	***	***	+	-	*	-	*	**	-	-	++	*
	B15.11	****	-	-	***	***	-	-	*	-	*	***	-	-	++	**
bricks made with ceramic sludge	FM	****	-	-	**	**	-	-	-	*	**	**	-	-	-	****
	B_PIR	****	-	-	*	***	-	-	+	*	***	***	-	-	-	**

		²²⁶ Ra (Bq/kg)	σ%	²³² Th (Bq/kg)	σ%	⁴⁰ K (Bq/kg)	σ%	U (ppm)	σ	Th (ppm)	σ	K (wt.%)	σ	I	I _α	Ra_eq (Bq/kg)	
raw materials	LG	31	11	37	7	526	3	3	-	9	-	2	-	0.47	0.16	125	
	LRS	29	17	34	10	633	6	2	-	8	-	2	-	0.48	0.14	126	
	LRSS	50	12	59	10	716	6	4	-	14	1	2	-	0.70	0.25	189	
	LRSSF	34	21	44	7	491	4	3	1	11	-	2	-	0.50	0.17	135	
	SS	-	-	-	13	279	6	-	-	1	-	1	-	-	-	30	
	TR	52	6	50	3	1210	2	4	-	12	-	4	-	0.82	0.26	216	
	F	-	-	<8	-	<58	-	-	-	-	-	-	-	-	-	-	-
	PIR	120	6	41	6	511	6	10	1	10	1	2	-	0.78	0.60	219	
	MN	-	-	<7	-	<47	-	-	-	-	-	-	-	-	-	-	-
commercial bricks	GP	45	14	47	9	700	3	4	1	11	1	2	-	0.62	0.22	161	
	N	29	17	43	7	654	6	2	-	11	1	2	-	0.53	0.15	137	
	RSS	41	14	52	7	757	3	3	-	13	1	2	-	0.65	0.21	168	
	R6	41	13	50	6	719	3	3	-	12	1	2	-	0.62	0.20	162	
	RS	36	17	44	6	755	2	3	1	11	1	2	-	0.60	0.18	151	
	RCF	43	13	46	7	666	3	3	-	11	1	2	-	0.60	0.21	156	
bricks made with trachyte waste	B5.9	55	12	56	8	1016	6	4	1	14	1	3	-	0.80	0.27	206	
	B5.10	50	11	43	7	614	3	4	-	11	1	2	-	0.59	0.23	155	
	B5.11	47	17	66	8	1000	6	3	1	16	1	3	-	0.82	0.24	212	
	B10.9	46	7	45	4	663	2	4	-	11	1	2	-	0.60	0.23	157	
	B10.10	51	12	44	8	693	3	4	-	11	1	2	-	0.62	0.25	163	
	B10.11	47	16	44	9	843	6	4	1	11	1	3	-	0.66	0.23	169	
	B15.9	46	10	43	6	689	3	4	-	11	1	2	-	0.59	0.23	155	
	B15.10	46	1	53	9	761	6	4	-	13	1	2	-	0.67	0.23	175	
	B15.11	47	17	66	8	1000	6	4	-	10	1	2	-	0.61	0.26	160	
bricks made with ceramic sludge	FM	40	12	54	8	696	3	3	0.40	13	1	2	-	0.64	0.20	167	
	B_PIR	55	9	46	12	599	6	4	0.41	11	1	2	-	0.61	0.28	163	

		Exhalation rate Q_A (Bq/d)	Surface exhalation rate E_a (Bq/d·m ²)	Mass exhalation rate E_m (Bq/d·kg)	Emanation coefficient η
commercial bricks	GP	0.014	1.28	0.133	0.016
	N	0.019	1.87	0.179	0.034
	RSS	0.017	2.84	0.176	0.023
	R6	0.084	8.58	0.803	0.109
	RS	0.016	1.65	0.153	0.024
	RCF	0.000	0.00	0.000	0.000
bricks made with trachyte waste	B5.9	0.040	3.64	0.321	0.032
	B5.10	0.015	0.96	0.143	0.016
	B5.11	0.003	0.26	0.024	0.003
	B10.9	0.029	2.96	0.275	0.033
	B10.10	0.034	3.35	0.310	0.034
	B10.11	0.024	2.80	0.266	0.031
	B15.9	0.030	2.89	0.250	0.030
	B15.10	0.013	1.52	0.113	0.014
B15.11	0.023	2.31	0.206	0.022	
bricks made with ceramic sludge	FM	0.028	2.84	0.282	0.039
	B_PIR	0.022	2.23	0.222	0.022

		ε_{tot} (%)	ρ_a (kg/m ³)	ρ_r (kg/m ³)	$\varepsilon_{<0.1\mu\text{m}}$ (%)	$\varepsilon_{<1\mu\text{m}}$ (%)	$\varepsilon_{>1\mu\text{m}}$ (%)	$\varepsilon_{0.1-1\mu\text{m}}$ (%)	S_{aBET}	S_{aMIP}	$S_{\text{aMIP}<0.05\mu\text{m}}$	$S_{\text{aMIP}<0.5\mu\text{m}}$
commercial bricks	GP	47.45	1400	2680	0.62	46.31	1.14	45.69	2.54	2.04	0.03	0.11
	N	46.87	1500	2870	0.83	46.02	0.86	45.18	4.33	2.57	0.04	0.10
	RSS	38.83	1540	2550	2.24	33.45	5.39	31.21	3.58	1.73	0.06	0.04
	R6	34.20	1700	2580	8.55	31.06	3.21	22.51	10.24	7.05	0.14	0.03
	RS	42.25	1540	2660	2.86	39.90	2.35	37.04	5.32	2.37	0.08	0.06
	RCF	35.85	1700	2580	1.13	24.05	11.80	22.92	1.56	1.20	0.02	0.26
Bricks made with trachyte waste	B5.9	25.22	1560	2090	3.16	20.37	4.86	17.21	2.11	2.94	0.12	0.02
	B5.10	38.10	1590	2570	1.30	22.24	15.93	20.94	2.21	1.63	0.06	0.02
	B5.11	34.40	1650	2520	0.93	16.80	17.67	15.87	0.63	0.90	0.05	0.02
	B10.9	27.50	1570	2170	5.11	20.53	7.03	15.42	1.93	3.26	0.12	0.01
	B10.10	38.39	1580	2560	1.73	23.39	15.00	21.66	0.98	1.57	0.07	0.02
	B10.11	19.40	1610	2000	0.00	11.36	8.04	11.36	0.58	0.27	0.01	0.01
	B15.9	23.22	1640	2140	4.10	19.17	4.05	15.07	1.48	3.44	0.13	0.01
	B15.10	36.97	1600	2550	2.57	23.07	13.89	20.50	0.95	2.44	0.08	0.02
	B15.11	27.58	1670	2310	0.53	14.68	12.90	14.15	0.50	0.60	0.03	0.01
bricks made with ceramic sludge	FM	49.57	1600	3100	2.61	47.21	2.36	44.60	1.99	1.07	0.08	0.32
	B_PIR	41.98	1460	2520	0.54	24.02	17.96	23.48	2.31	1.81	0.04	0.24

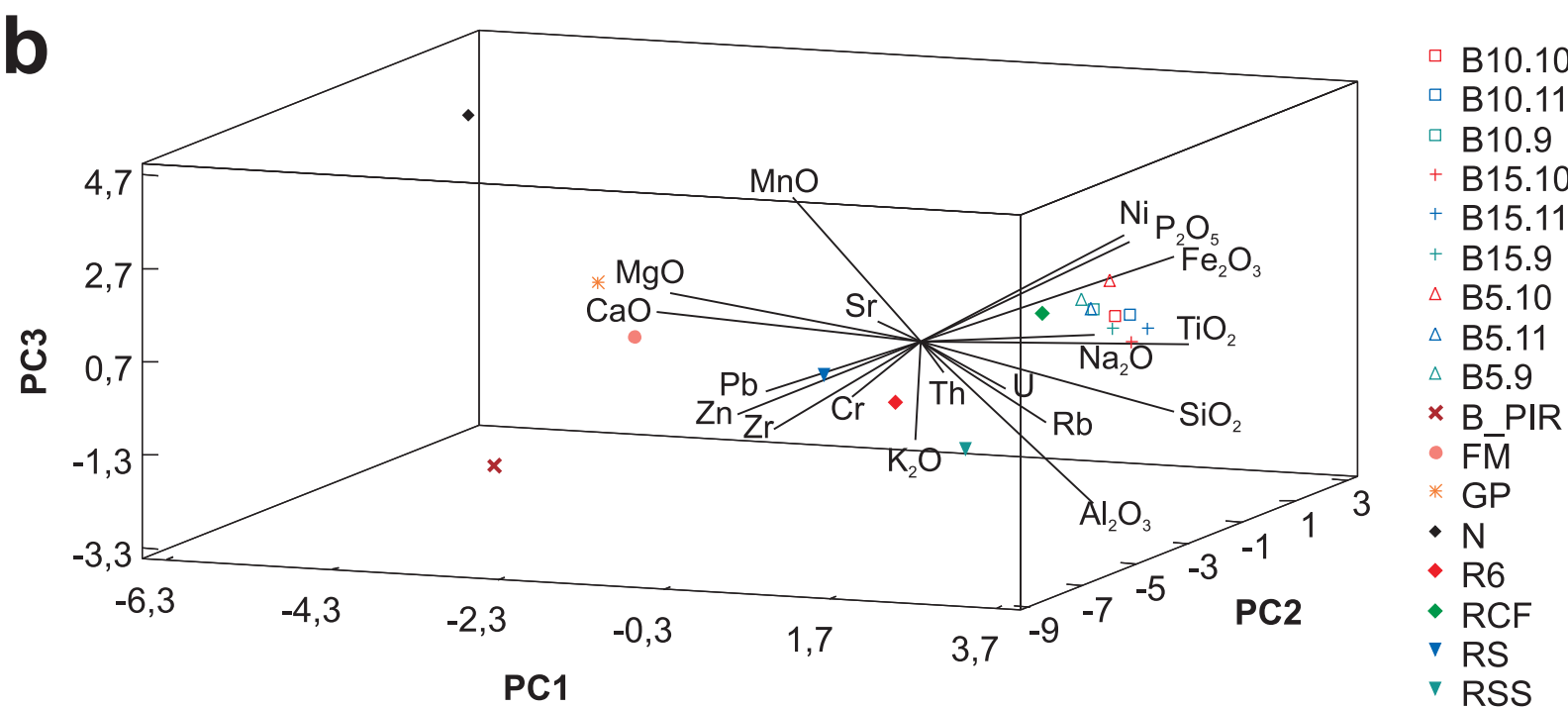
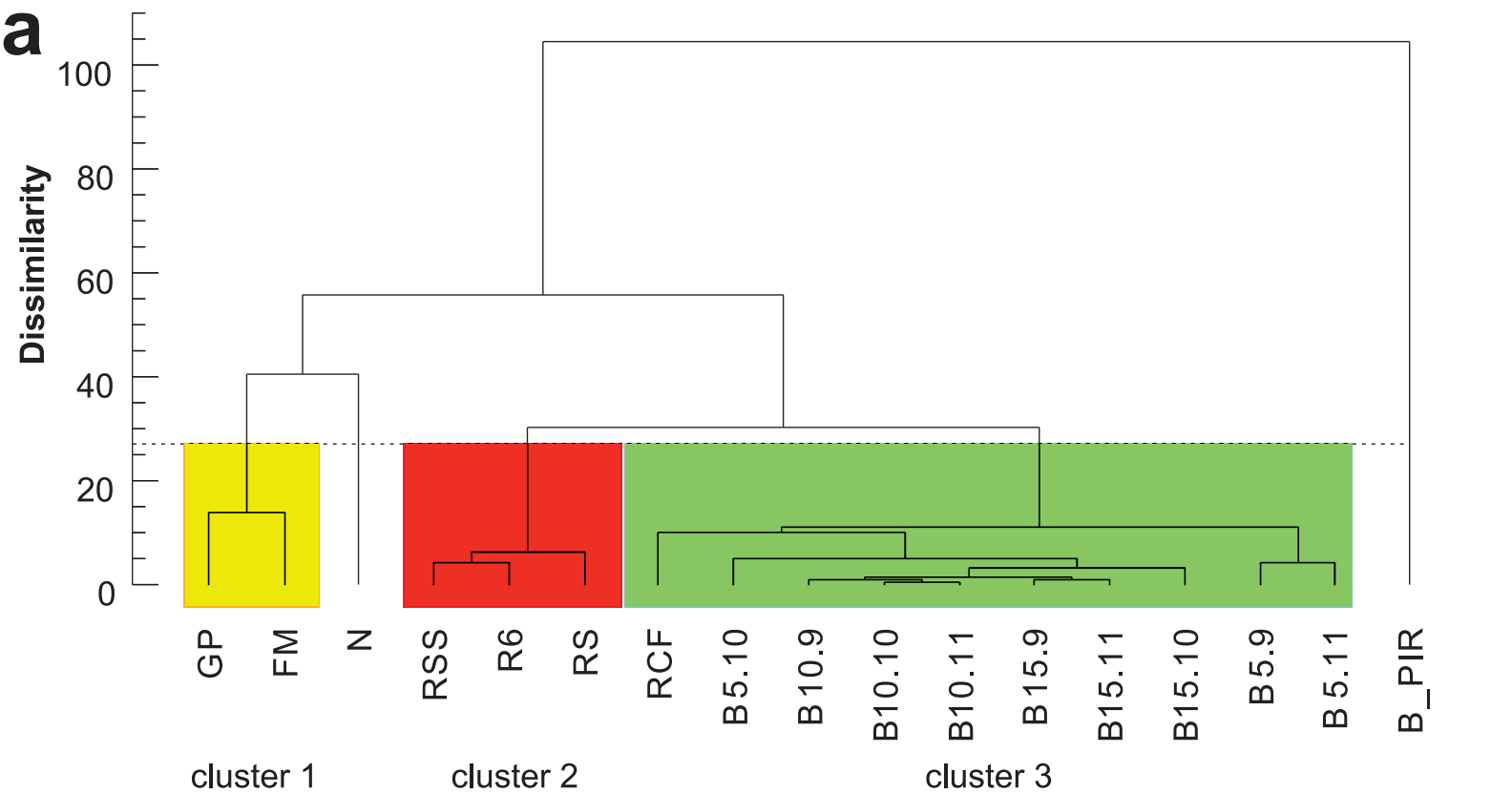


Figure 2

[Click here to access/download;Figure;Fig. 2.eps](#)

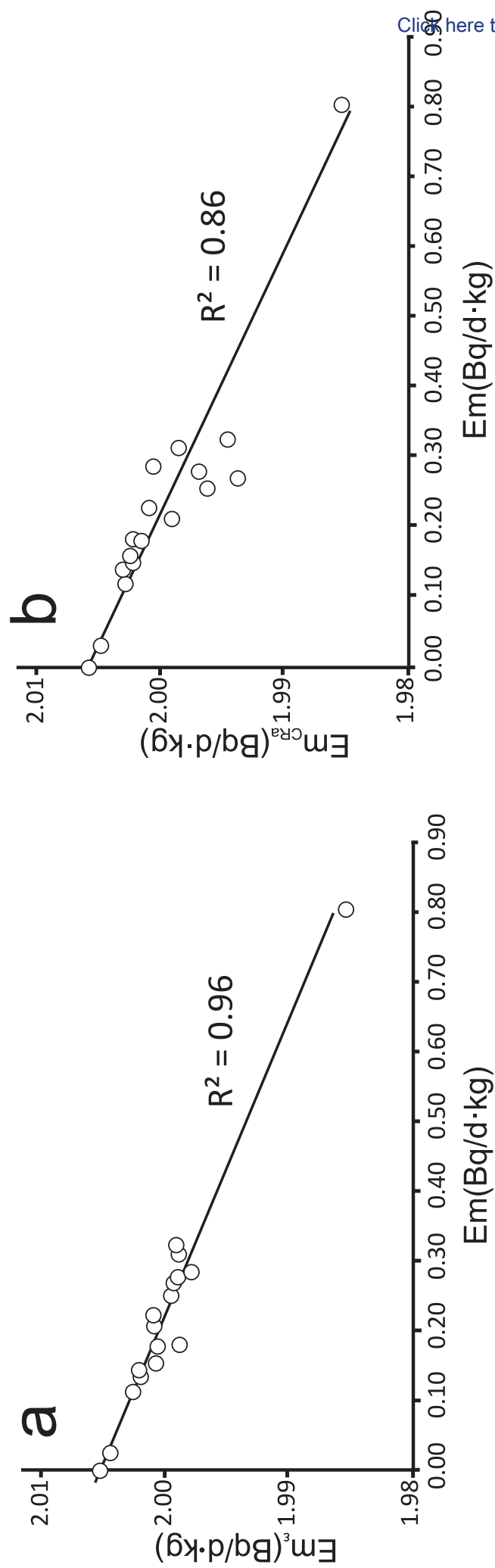


Figure 3

[Click here to access/download;Figure;Fig. 3.eps](#)

